Journal of Earthquake Engineering

ISSN: 1363-2469 (Print) 1559-808X (Online) Journal homepage: www.tandfonline.com/journals/ueqe20

Dynamic Characterization and Seismic Performance of a Fully-Floating Ceiling with Velcro-Secured Lay-in Tiles via Shake Table Tests

A. Tiwari , J. Bhatta , R. P. Dhakal, T. J. Sullivan , R. K. Shrestha , Z. Yan , G. A. MacRae , J. Yu , P. Xiang , M. Rashid , Y. Zhang , L. Jia , S. Ramhormozian , G. C. Clifton , P. Quenneville , G. Rodgers & X. Zhao

To cite this article: A. Tiwari , J. Bhatta , R. P. Dhakal, T. J. Sullivan , R. K. Shrestha , Z. Yan , G. A. MacRae , J. Yu , P. Xiang , M. Rashid , Y. Zhang , L. Jia , S. Ramhormozian , G. C. Clifton , P. Quenneville , G. Rodgers & X. Zhao (06 Apr 2026): Dynamic Characterization and Seismic Performance of a Fully-Floating Ceiling with Velcro-Secured Lay-in Tiles via Shake Table Tests, Journal of Earthquake Engineering, DOI: 10.1080/13632469.2026.2642761

To link to this article: https://doi.org/10.1080/13632469.2026.2642761

Published online: 06 Apr 2026.

JOURNAL OF EARTHQUAKE ENGINEERING
https://doi.org/10.1080/13632469.2026.2642761

Taylor & Francis
Taylor & Francis Group

Dynamic Characterization and Seismic Performance of a Fully-Floating Ceiling with Velcro-Secured Lay-in Tiles via Shake Table Tests

A. Tiwari[a], J. Bhatta[a], R. P. Dhakal[a], T. J. Sullivan[a], R. K. Shrestha[a], Z. Yan[b], G. A. MacRae[a], J. Yu[c], P. Xiang[c], M. Rashid[d], Y. Zhang[a], L. Jia[c], S. Ramhormozian[b], G. C. Clifton[e], P. Quenneville[e], G. Rodgers[f], and X. Zhao[c]

[a]Civil and Environmental Engineering, University of Canterbury, Christchurch, New Zealand; [b]Built Environment Engineering, Auckland University of Technology, Auckland, New Zealand; [c]College of Civil Engineering, Tongji University, Shanghai, China; [d]Silvester Clark, Palmerston North, New Zealand; [e]Civil and Environmental Engineering, University of Auckland, Auckland, New Zealand; [f]Mechanical Engineering, University of Canterbury, Christchurch, New Zealand

ABSTRACT

Grid-and-tile suspended ceilings, commonly used in commercial buildings, have historically suffered significant damage during earthquakes leading to financial losses, business disruption, and life-safety hazards. This study investigates the dynamic characteristics and seismic performance of a fully-floating ceiling, a low-damage ceiling concept that incorporates Velcro-secured lay-in tiles. In this system, Velcro tape, a novel addition, is used to secure the tiles to the Tees, aiming to prevent tile dislodgement during shaking. The ceiling was installed on the second storey of a three-storey steel-framed building and tested on a shake table under unidirectional and bidirectional shaking. These tests were part of the RObust BUilding SysTem (ROBUST) project, conducted at the International Joint Research Laboratory of Earthquake Engineering at Tongji University, China. During the experiments, the fully-floating ceiling was subjected to peak floor accelerations of up to 0.60 g simultaneously in the longitudinal and transverse directions (vector resultant of 0.85 g). The system exhibited median fundamental modal periods of 0.31 s and 0.40 s in the two orthogonal horizontal directions, with median damping ratios ranging from 2.39% to 3.63%. The peak displacement reached 40.6 mm, and the ceiling remained insensitive to torsional effects. The median acceleration amplification factor in the horizontal directions was 2.16, and the maximum vertical peak component ceiling acceleration was 1.01 g. No pounding between sprinkler heads and lay-in tiles was observed. Throughout the testing program, no damage was observed. These findings highlight the potential of the fully-floating ceiling as a low-damage, seismically resilient solution for use in buildings located in earthquake-prone regions.

ARTICLE HISTORY
Received 17 November 2025
Accepted 1 March 2026

KEYWORDS
Fully-floating ceiling; lay-in tiles; Velcro tape; shake table; low-damage ceiling; dynamic characterization

CONTACT A. Tiwari aasish.tiwari@pg.canterbury.ac.nz Civil and Environmental Engineering, University of Canterbury, Private Bag 4800, Christchurch 8140, New Zealand

1. Introduction

Non-structural or non-skeletal elements (NSEs) are essential for ensuring the functionality of buildings and facilities and account for a considerable share of the total building cost (Bradley et al. 2009; R. Dhakal 2024; Khakurel et al. 2020; Taghavi and Miranda 2003). In recent decades, developments in earthquake engineering have increasingly focused on innovative design solutions for NSEs to limit damage and, consequently, minimize repair costs, prevent injuries or casualties, and ensure post-earthquake functionality of buildings (Bhatta and Dhakal 2026; Bhatta et al. 2022; Bianchi et al. 2021; Ditommaso et al. 2025; Maneetes and Memari 2014; Mulligan, Sullivan, and Dhakal 2022; Pinelli et al. 1996; Pourali et al. 2017; Yagi et al. 2022).

Among various NSEs, suspended ceilings are widely used systems that conceal mechanical and electrical services such as pipes, ducts, and cable trays in their plenum, while enhancing aesthetics and maintaining acoustics. The damage to suspended ceilings during past earthquakes has been substantial, leading to significant financial losses, operational downtime, and, in some instances, loss of life (R. P. Dhakal 2010; R. P. Dhakal, MacRae, and Hogg 2011; Motosaka and Mitsuji 2012).

Suspended ceilings are broadly categorised as grid-and-tile suspended ceilings or plasterboard suspended ceilings. In grid-and-tile suspended ceilings, lay-in tiles are generally placed, within a grid formed by the intersection of main-Tees and cross-Tees, without being attached to the Tees. In contrast, plasterboard suspended ceilings involve fastening plasterboard panels underneath the furring channels using screws. Consequently, the Tees remain exposed in grid-and-tile suspended ceilings, but furring channels are concealed in plasterboard suspended ceilings.

A typical grid-and-tile ceiling comprises a grid formed by the crossing of main-Tees and cross-Tees, wall angles, lay-in tiles and a gravity support system of hanger wires as shown in Fig. 1. In New Zealand, two types of grid-and-tile ceilings are commonly used, differing in how the seismic forces developed within the ceiling are transferred to adjacent structural elements (such as beams or slabs) or non-structural elements (such as partition walls). The commonly used types are perimeter-fixed and braced ceilings, as shown in Fig. 2a,b, respectively.

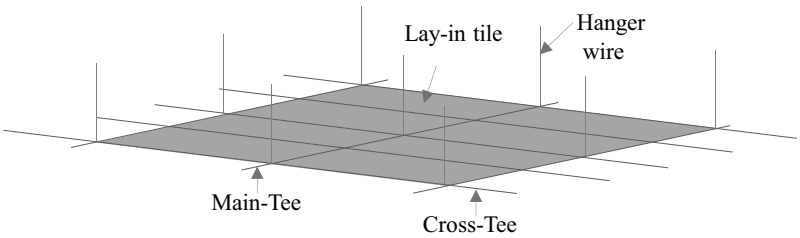

Figure 1. A typical grid-and-tile ceiling.

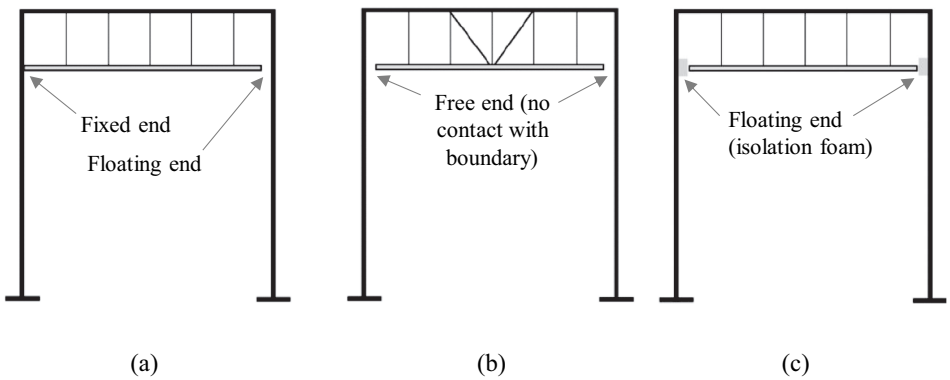

Figure 2. Categories of suspended ceiling systems: (a) perimeter-fixed (typical); (b) braced (typical); (c) fully-floating (low-damage); redrawn from Rashid (2022).

In perimeter-fixed ceiling, the ends of Tees are fixed to wall angles on two adjacent sides of the perimeter using rivets or screws, while the Tees on the remaining two sides rest on the wall angles without being attached. This allows the Tees to float along the slots of seismic clips. The major demand in this system is the axial force developed along the Tees, which is resisted by the rivets or screws. These forces are then transferred to the wall angles, which are secured to the walls.

In contrast, in braced ceiling, the ends of main-Tees and cross-Tees at the perimeter are attached to wall angles using rivets or screws. The wall angles are not connected to the surrounding walls or beams, and a sufficient gap is provided to ensure that no ceiling edges come into contact with the surrounding walls or beams, even during lateral shaking. Thus, all ceiling edges remain free. Lateral forces in this system are transferred to the floor above through the braces.

In addition to the above systems, a novel fully-floating grid-and-tile ceiling, the focus of this research (hereafter referred to as fully-floating ceiling), was proposed by Pourali et al. (2017) and is shown in Fig. 2c. The attachment of main-Tees and cross-Tees to the wall angles is similar to that in braced ceilings. However, the gaps between the wall angles and the surrounding walls are filled with compressible isolation foam. This foam prevents the ceiling from pounding against the walls and allows controlled floating of the ends. Unlike the lateral force resistance provided by braces in braced ceilings or rivets or screws in perimeter-fixed ceilings, this system uses isolation foam to control the lateral movement. The use of isolation foam contributed to the development of a low-damage ceiling solution (Pourali et al. 2017).

Pourali et al. (2017) reported promising results from unidirectional shake table tests on a fully-floating ceiling but emphasized the necessity of further research under multi-directional seismic loading. Moreover, Ryu and Reinhorn (2019) reported that ceilings subjected to multi-directional seismic loading are more vulnerable than those subjected to unidirectional loading. Therefore, this study investigates the dynamic characteristics and the seismic performance of a fully-floating ceiling under multi-directional loadings. For this, the ceiling was installed on the second-storey of a full-scale three-storey steel-framed structure tested on a shake-table under unidirectional and bidirectional loadings as a part of ROBUST project. This study aims to investigate (a) the natural frequencies, (b) damping ratios, (c) seismic responses, and (d) acceleration amplification factors of the tested fully-floating ceiling. It is noted that certain NSEs, such as infill walls, are known to influence the dynamic response of structures as shown in past works Su et al. (2005) and Ditommaso, Lamarucciola, and Ponzo (2024), among others. However, there is no evidence that lightweight ceiling systems affect structural performance beyond their contribution to the overall seismic mass; therefore, the influence of the ceiling on the dynamic response of the structure is not considered in this study.

2. Background

2.1. Seismic Performance of Suspended Ceilings with Lay-in Tiles

Damage to grid-and-tile ceilings during past earthquakes has been reported in various forms, including failure at main-Tee and cross-Tee intersections; buckling, twisting, and breaking of Tees due to excessive compression; disconnection of Tees from wall angles; main-Tee splice failure; edge and perimeter fixing failures; dislodgement and dropping of tiles; and pounding between lay-in tiles and sprinkler systems (R. P. Dhakal, MacRae, and Hogg 2011; R. P. Dhakal et al. 2016; Gilani et al. 2010).

2.2. Previous Studies in Suspended Ceilings with Lay-in Tiles

Several researchers (R. P. Dhakal et al. 2016; Ryu and Reinhorn 2019; Soroushian, Maragakis, and Jenkins 2015; Zaghi et al. 2016) have sought to identify vulnerabilities and improve the seismic performance of conventional ceiling systems, such as perimeter-fixed and braced ceilings.

Despite extensive research on conventional ceiling systems, studies specifically focusing on fully-floating ceiling systems remain limited. However, a few investigations have examined ceilings suspended freely by hanger wires, without stiff connections to peripheral walls, and without isolation foam (hereafter referred to

as early variant of fully-floating ceiling). For example, an early report from the 1980s (ANCO-Engineers-Inc 1983) found that an early variant of fully-floating ceiling experienced lower peak accelerations, but higher peak displacements compared to braced ceilings supported by 45-degree splay wires. Similarly, Yao (2000) conducted shaking table tests on an early variant of fully-floating ceiling in Taiwan and found that the ceiling period could be reliably predicted using simple pendulum theory, a finding later supported by Robson et al. (2014).

Pourali et al. (2017) proposed a low-damage concept by adding compressible foam material (referred to as isolation foam) between the edges of the ceiling (4550 mm by 2150 mm) and the surrounding timber beam (as shown in Fig. 3) to limit lateral displacement. The lay-in tiles were placed over the Tees without any connection along their seatings. Through unidirectional shake table experiments using a wide range of sinusoidal and recorded ground motions, Pourali et al. (2017) found that the isolation foam was effective in limiting the lateral displacement of the ceiling from 100 mm (recorded on early variant of fully-floating ceiling) to 20 mm (recorded on fully-floating ceiling). The only failure observed was the dislodgement of a single lay-in tile in the ceiling variant incorporating isolation foam under sinusoidal tests (shown in Fig. 4).

Jun et al. (2022) conducted shake table tests on an early variant of the fully-floating ceiling (3870 mm by 3870 mm). The lay-in tiles were simply placed over the Tees without any connection along their seatings. This ceiling system was subjected to maximum peak floor accelerations of 1.43 g, 1.03 g, and 0.38 g in the longitudinal, transverse, and vertical directions, respectively. Under this level of seismic demand, approximately 30% of the lay-in tiles were dislodged.

2.3. Lay-in Tile Dislodgement and its Prevention

According to FEMA356 (2000), the dislodgement of an isolated lay-in tile is acceptable to meet the Operational Level. However, if a tile dislodgement occurs, the in-plane stiffness of the ceiling system is reduced, leading to increased deflection of Tees. This, in turn, can cause further dislodgement of lay-in tiles and additional Tee failures creating a "domino effect," causing the collapse of the system as noted by Ryu and Reinhorn (2019) and discussed by Browne, Long, and Stanway (2024). Therefore, preventing the dislodgement of lay-in tiles is essential to ensuring the ceiling system remains operational.

Badillo-Almaraz, Whittaker, and Reinhorn (2007) investigated the use of retainer clips to prevent the dislodgement of lay-in tiles through dynamic testing of suspended ceiling systems using a full-scale earthquake simulator. The use of retainer clips significantly improved ceiling performance by reducing the likelihood of lay-in tile collapse. However, these clips increased inertial loads on the Tees, resulting in damage of the Tees at lower levels of shaking. Lay-in tile collapse in systems with the retainer clips was primarily due to Tee failures. Additionally, the retainer clips complicate access to plenum space making maintenance of services more challenging as mentioned by Browne, Long, and Stanway

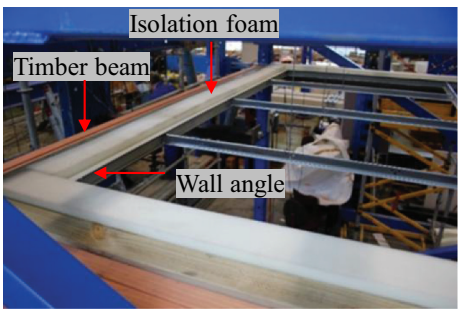

Figure 3. Isolation foam placed between the ceiling and the timber beam (Pourali et al. 2017).

Figure 4. Lay-in tile dislodgement under sinusoidal test observed on a fully-floating ceiling (Pourali et al. 2017).

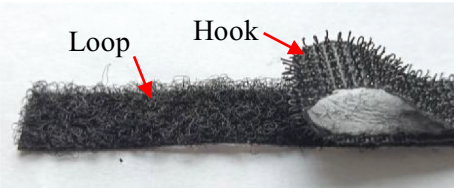

Figure 5. Hook and loop components of Velcro tape.

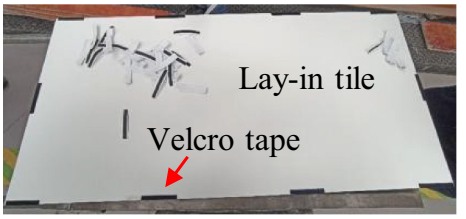

Figure 6. Velcro tape applied to a lay-in tile.

(2024). Thus, there is a need to identify a simple and practical method to restrain lay-in tiles while allowing easy removal and reinstallation for maintenance. The authors of this study proposed using hook-and-loop tape (Velcro tape) to secure lay-in tiles to the Tees.

Velcro tape is a fastening system consisting of two distinct components: the hook side and the loop side (as shown in Fig. 5). The hook component is made up of numerous small, stiff hooks typically formed from nylon or polyester, while the loop component consists of soft, pliable loops made of woven or knitted fabric. When pressed together, the hooks engage with the loops to create a mechanical bond that can be repeatedly fastened and released (Velcro-Brand n.d.). The authors of this study believe using Velcro tape to secure lay-in tiles to the Tees along their seatings can reduce the risk of dislodgement, enhance in-plane stiffness, and ultimately improve the seismic performance of the system. A lay-in tile secured to Tees with Velcro tape is hereafter referred to as Velcro-secured lay-in tiles. Accordingly, the ceiling system evaluated in this study features Velcro-secured lay-in tiles (as shown in Fig. 6) and represents the first experimental investigation of a fully-floating ceiling system featuring Velcro-secured lay-in tiles.

3. Test Setup and Instrumentation

A series of shake table tests on a full-scale, three-storey steel frame building was recently completed under a New Zealand-China collaborative research program, the ROBUST project. The tests were conducted at the International Joint Research Laboratory of Earthquake Engineering (ILEE) at Jiading Campus, Tongji University, Shanghai, China. The primary objective of the project was to investigate the seismic behaviour of low-damage solutions for both structural and non-structural systems (R. P. Dhakal et al. 2020; G. A. MacRae et al. 2020). The low-damage, three-story steel-framed building consisted of two bays in the longitudinal (NS/X) direction and one bay in the transverse (EW/Y) direction. It featured interchangeable seismic-resisting structural configurations and a composite flooring system (comFlor deck) using ComFlor®80 (Steel & Tube 2016). Seismic-resisting systems were of either moment frames, braced frames, rocking frames, or rocking columns (Yan et al. 2023). The structure measured 7250 mm between column centres in the X-direction, 4750 mm in the Y-direction, and had a 3000 mm inter-storey height. The building was designed as an office building for Wellington, with a zone factor of 0.40, in accordance with NZS1170.5 (2016). Suspended ceilings, along with other NSEs, were tested in the last testing sequence of the test series, referred hereafter as the NSEs Test.

3.1. Structural System for the NSEs Test

In the NSEs Test, the seismic-resisting system in the longitudinal (NS/X) direction comprised a moment resisting steel frame (MRSF) incorporating the optimised sliding hinge joints (OSHJs) at the beam-to-column connections. The OSHJs were implemented in bay 2 only (encircled in Fig. 7), while bay 1 consisted of pinned beam-to-column connections. In the transverse (EW/Y) direction, V-braced concentrically braced frames (CBFs) were adopted as shown in Fig. 8. Symmetric friction connections (SFCs) using partially deflected Belleville Springs were used at the brace-to-gusset plate connections. The details of the structural system can be found in (MacRae et al., 2024; Yan et al., 2024; Yan et al., 2023).

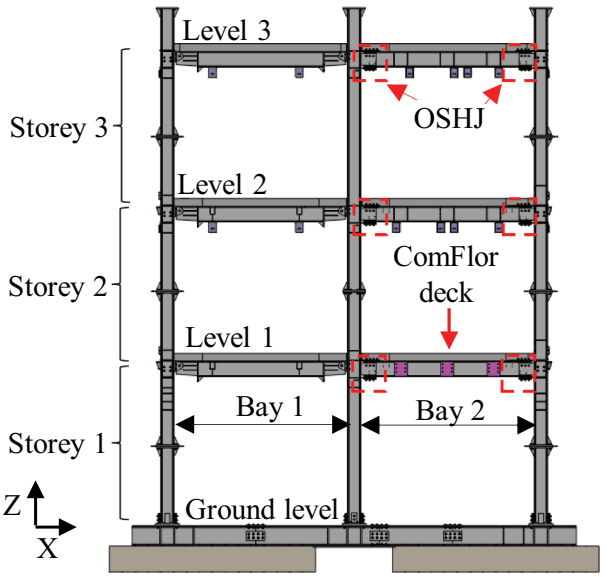

Figure 7. Schematic of the steel test structure (longitudinal (NS/ X) direction) showing OSHJ encircled; redrawn from Yan et al. (2023).

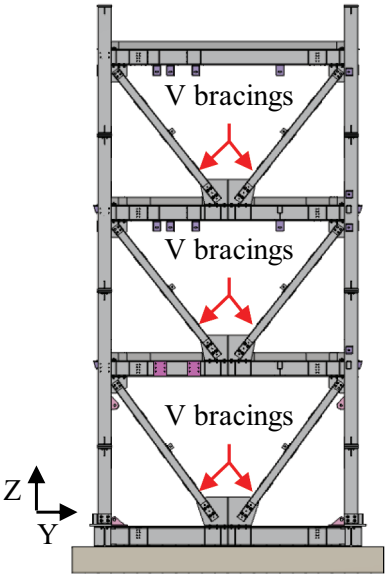

Figure 8. Schematic of the steel test structure (transverse (EW/ Y) direction) showing V bracings; redrawn from Yan et al. (2023).

The accelerations and displacements of the structural system were recorded using accelerometers and string-potentiometers respectively at each floor level. Two accelerometers were installed in the longitudinal (NS/X) direction and two in the transverse (EW/Y) direction at each level, including the ground level, and levels 1, 2, and 3. Additionally, one accelerometer was installed in the vertical (Z) direction at each of levels 1, 2, and 3. To measure the displacements of the structural system, two string-potentiometers were installed in each X and Y direction at every floor level. Fig. 9 illustrates the instrumentation plan at Level 2, from which the fully-floating ceiling was suspended.

3.2. Fully-Floating Ceiling System

The fully-floating ceiling of dimension 6670 mm by 4300 mm (shown in Fig. 10) was installed on the entire second storey (shown in Fig. 11). In this ceiling, the main-Tees were spaced 1200 mm apart, while the cross-Tees, positioned between the main-Tees, were spaced at intervals of 600 mm. The main-Tees and the cross-Tees were enclosed at the perimeter using wall angles. Ten Velcro tapes of 100 mm in length and 10 mm width were used to attach a lay-in tile of size 600 mm by 1200 mm (shown in Fig. 6 and Fig. 10). Fig. 12 presents a concise overview of the installation steps for the fully-floating ceiling system. Table 1 describes the components used (shown in Fig. 10), including the main-Tees, cross-Tees, wall angles, lay-in tiles, and hanger wires.

The ceiling was suspended at a plenum depth of 700 mm from the bottom of the ComFlor deck using hanger wires, which were distributed approximately symmetrically as shown in Fig. 10. Fig. 13 shows the boundary condition of this ceiling at its edges. The ends of the Tees of the ceiling were connected to the wall angle using seismic clips, as shown in Fig. 14. The Tees were secured to the seismic clips with two screws (M4 and 20 mm in length), and the seismic clips were secured to the wall angles using two screws of the same size. Instead of directly screwing the Tees to the wall angles, the Tees were screwed to seismic clips, which were then screwed to the wall angles. This configuration was adopted to prevent friction during ceiling displacement, which could occur if the Tees were connected

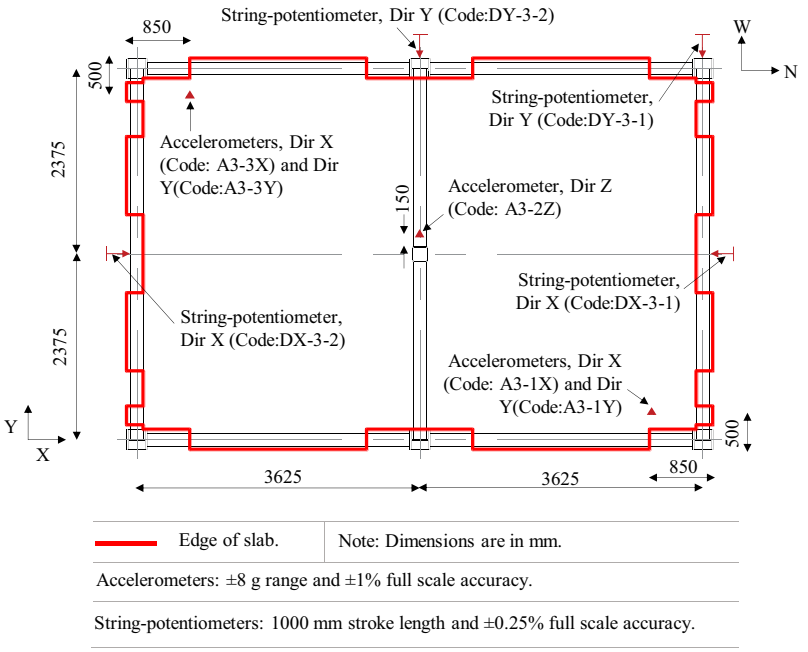

Figure 9. Instrumentation plan used at level 2 floor.

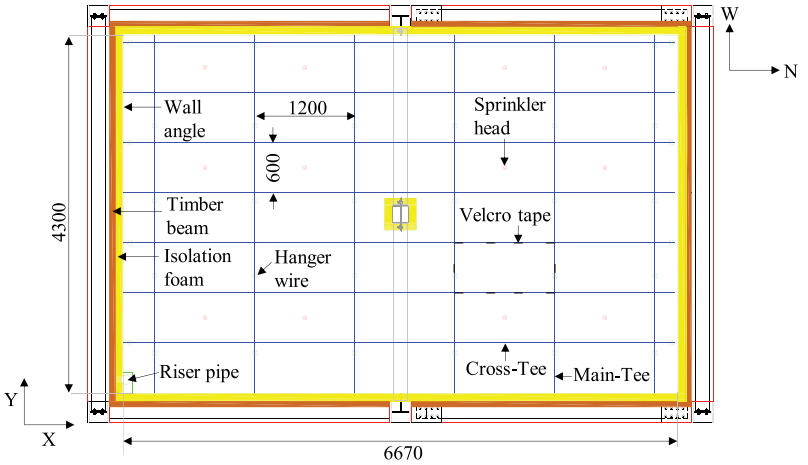

- Dimensions are in mm.
- 600 mm x 1200 mm lay-in tile secured to Tees with 10-100 mm long Velcro tape.

Figure 10. Fully-floating ceiling suspended from level 2 of the tested building redrawn from Rashid (2022).

directly to the wall angles. In such direct connections, the tips of the screws may contact the perimeter channel, introducing friction that could restrict free movement. To hold the isolation foam (100 mm by 90 mm), which is similar to the isolation foam used by Pourali et al. (2017), perimeter channels measuring 150 mm by 150 mm by 2 mm were nailed to the timber beams.

To ensure the floating of the ceiling, a 20 mm vertical gap was provided between the wall angle and the perimeter channel (shown in Fig. 15), and a horizontal gap was provided between the isolation foam and the wall angle. Despite efforts to maintain a horizontal gap of 10 mm between the ceiling and the isolation foam, this could not be achieved due to the following reasons, resulting in a gap that ranged from 0 to 10 mm (shown in Fig. 16):

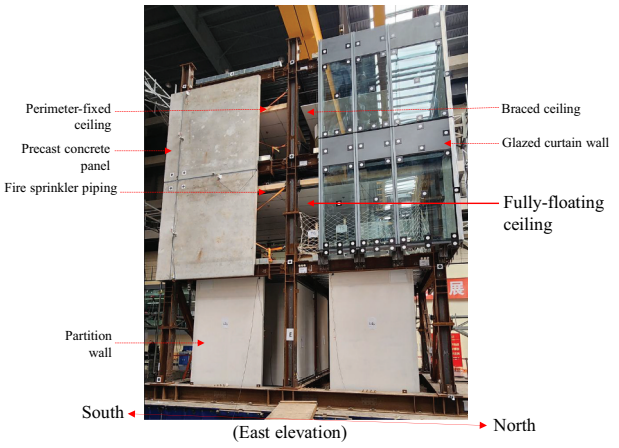

Figure 11. ROBUST tested structure with the fully-floating ceiling, along with other NSEs.

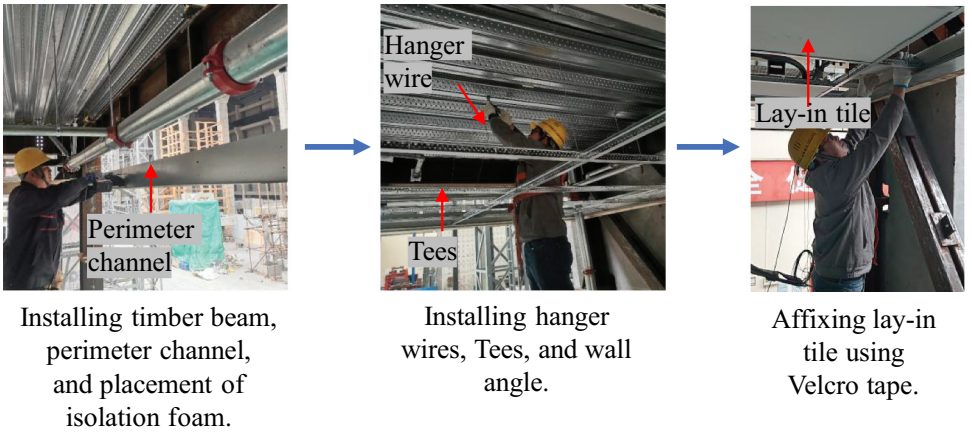

Figure 12. Overview of installation steps of the fully-floating ceiling.

Table 1. Typical details of components of suspended ceilings.

Component	Product Name	Material	Dimensions
Main-Tee	Armstrong Peakform Prelude 24 mm	Hot-dipped galvanised steel	24 mm (w) × 43 mm (h) × 3600 mm (l)
Cross-Tee	Armstrong Peakform Cross Tee 1200	Hot-dipped galvanised steel	24 mm (w) × 35 mm (h) × 1200 mm (l)
Wall angle	Armstrong Peakform Wall Angle	Hot-dipped galvanised steel	22 mm(w) × 22 mm (h) × 3000 mm (l)
Tile	Armstrong Ultima Board	Mineral Fibre (5.21 kg/m^2 of 19 mm thick)	1200 mm (l) × 600 mm (w) × 19 mm (t)
Hanger wire	–	Galvanised soft-annealed steel	Diameter of 2.68 mm

w: width; h: height; l: length; t: thickness.

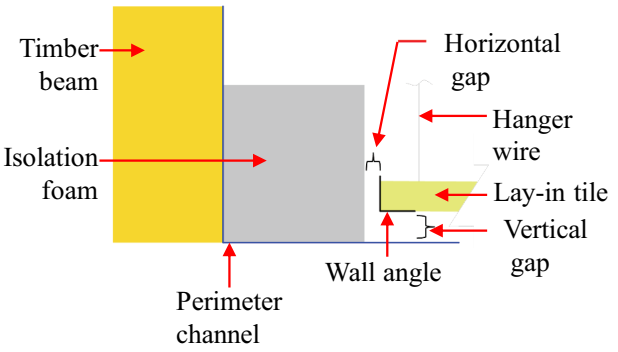

Figure 13. Schematic representation of the boundary condition of the fully-floating ceiling at the edges (side-sectional view).

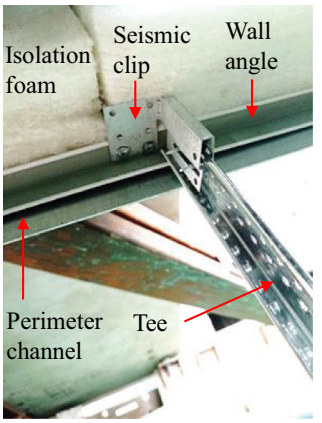

Figure 14. Connection of the Tee with the wall angle.

(1) The isolation foam mass was manually cut to a target cross-sectional dimension of approximately 90 mm by 100 mm. However, the resulting sections lacked uniformity, with dimensions often exceeding 90 mm and 100 mm (shown in Fig. 17).
(2) The tips of the screws connecting the seismic clips to the wall angle interfered with the isolation foam, causing it to hook onto the foam sections (shown in Fig. 18).
(3) The isolation foam had to be tightly packed in the corners of the ceiling, and at locations where installation of the perimeter channel was particularly challenging, such as around columns (shown in Fig. 19) and the riser pipe.

In the study on conventional ceilings by Soroushian et al. (2012), sprinkler heads fitted to rigid droppers caused tearing of the lay-in tiles, even though oversized sleeves (50 mm) were provided around the sprinkler heads. In contrast, no damage was observed in cases where flexible droppers were used. Given that fully-floating ceilings are more displacement-sensitive than conventional ceilings (Pourali et al. 2017), the use of rigid droppers could lead to even greater relative displacement and potential damage, such as tearing of lay-in tiles. Therefore, flexible droppers were adopted in this study, based on the assumption that they would be more compatible with the fully-floating ceiling (shown in Figs. 20 and 21). These droppers were clamped to Tees using support bar as shown in Fig. 20.

Eleven sensor channels, with a sampling frequency of 256 Hz, were employed to measure the accelerations and displacements of the fully-floating ceiling. The location and basic specifications of accelerometers and string-potentiometers are shown in Fig. 22. All sensors were securely affixed to the Tees at their respective locations. Representative photos of the instrumentation, including string-potentiometer D18 and accelerometers A12-X, A12-Y, and A12-Z are shown in Fig. 23.

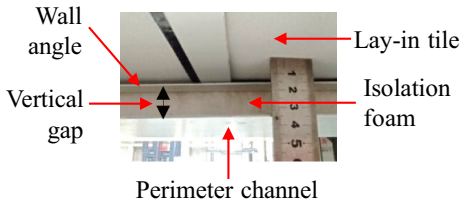

Figure 15. Vertical gap between the wall angle and the perimeter channel.

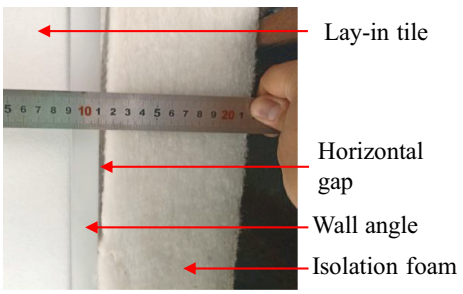

Figure 16. Horizontal gap between the wall angle and the isolation foam.

Figure 17. Preparation of isolation foam.

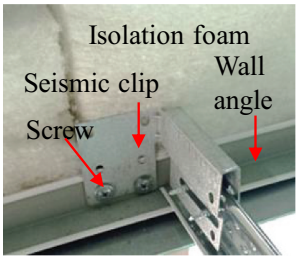

Figure 18. The tip of screws interfering with the isolation foam.

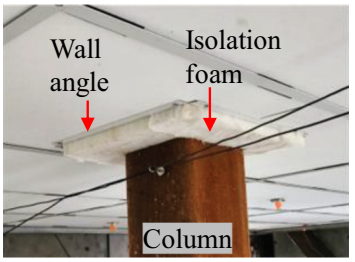

Figure 19. Isolation foam packed in the gap between the ceiling and the central column.

3.3. Shaking Sequence Used in NSEs Test

A single earthquake record was chosen from the Imperial Valley, El Centro 1940, Array #9 station ground motions. This record was subsequently scaled to various intensity levels to match the target response spectrum over the period range of interest (0.08 s to 1.97 s). The selection criteria and scaling methods of the chosen table motion are thoroughly explained in (Bagheri 2022). In the NSEs Test, the tested building was subjected to progressively increased earthquake intensity (listed in Table 2), ranging from the Serviceability Limit State (SLS) to 1.2 times the Maximum Considered Earthquake (MCE). The structure was tested under unidirectional loadings (X and Y directions separately) and under bidirectional loadings (X and Y directions simultaneously). Additionally, bidirectional white noise, of 0.05 g, was applied before and after each loading sequence to detect any changes in the dynamic properties of the tested building.

3.4. Signal Processing and Data Acquisition

Acceleration and displacement data were acquired at a sampling frequency of 256 Hz. The acceleration records were detrended to eliminate the linear trend (zero-frequency DC component), while the

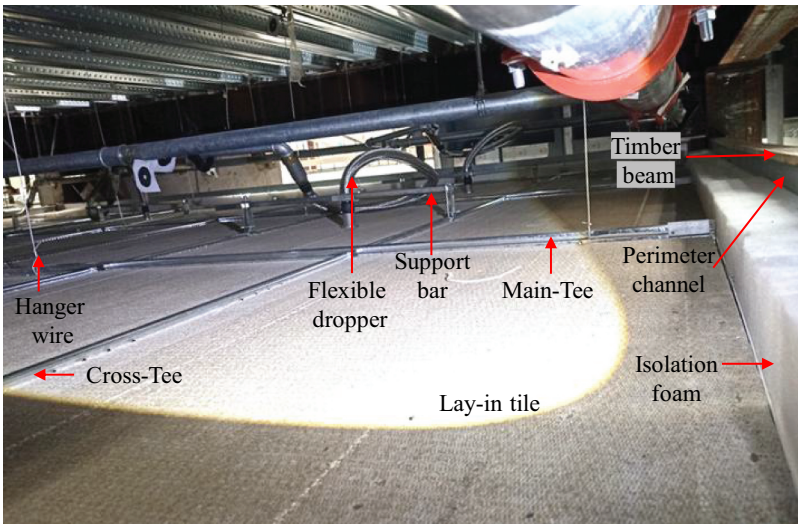

Figure 20. Photo of fully-floating ceiling in the plenum space.

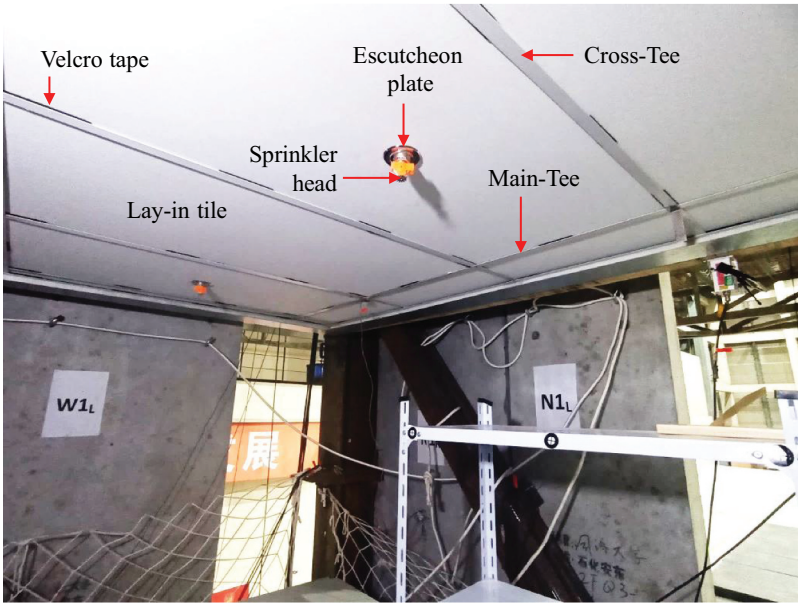

Figure 21. Photo of fully-floating ceiling as seen from bottom.

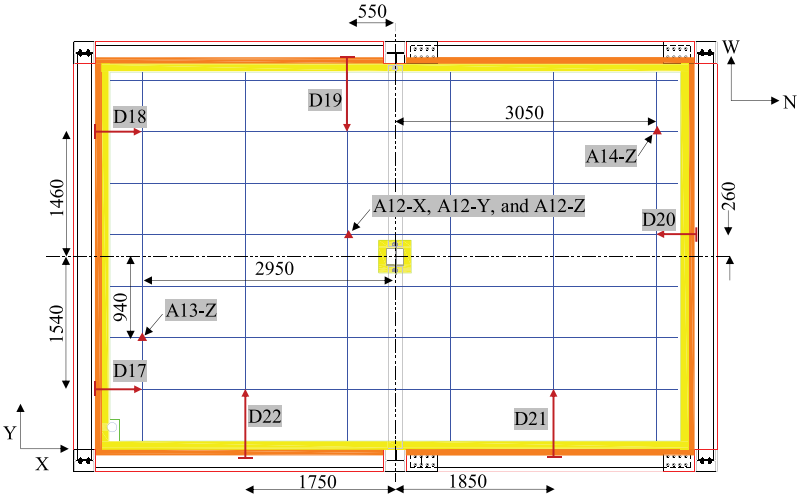

- Dimensions are in mm.
- A12-X, A12-Y, and A12-Z are unidirectional accelerometers along X, Y, and Z directions respectively.
- A13-Z, and A14-Z are unidirectional accelerometers along Z-direction.
- Accelerometers: ±5 g range, except A13-Z (±8 g range and ±1% full-scale accuracy).
- D17, D18, D19, D20, D21, and D22 are string-potentiometers; 200 mm stroke length and ±0.25% full-scale accuracy.

Figure 22. Instrumentation used in the fully-floating ceiling.

displacement records were baseline-corrected. Both the detrended acceleration and baseline-corrected displacement records were then filtered using a fourth-order low-pass Butterworth filter with a cutoff frequency of 50 Hz. The ceiling performance was also monitored through digital video recordings and a thorough post-shake physical inspection. The first inspection was conducted following a bidirectional loading intensity of 0.10 g. As the shaking intensity increased, inspections were

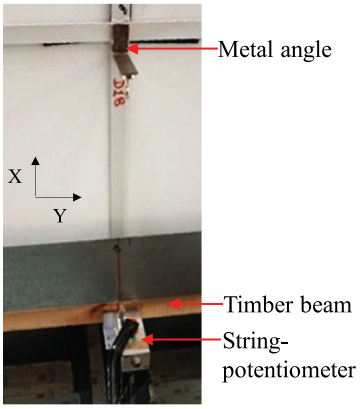

(a) String-potentiometer, D18.

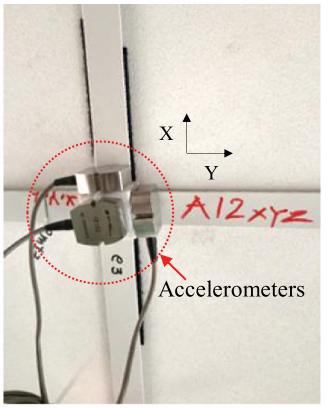

(b) Accelerometers, A12XYZ (i.e. A12-X, A12-Y, and A12-Z).

Figure 23. Representative photos of instrumentation in the fully-floating ceiling.

performed more frequently as listed in Table 2. Damage to individual components was documented by capturing detailed photos and videos, recording observations on inspection sheets, and physically measuring and marking the observed damage.

4. Experimental Results and Discussions

This section presents the experimental results and analysis for the dynamic characterization, including natural frequencies and damping ratios, and the seismic responses of the fully-floating ceiling, such as acceleration amplification factors, peak ceiling displacements, and torsional responses under the shaking sequences discussed under the previous section. In addition, the structural response, specifically the peak floor acceleration (PFA) of the floor from which the ceiling is suspended, is also reported. This PFA represents the seismic demand imposed on the fully-floating ceiling.

4.1. Peak Floor Acceleration: Demand on the Fully-Floating Ceiling

In the NSEs Test phase, ROBUST tested building was subjected to unidirectional and bidirectional shaking (listed in Table 2). The maximum intensities applied were 0.6 g unidirectional and 0.88 g bidirectional peak ground acceleration (PGA).

Peak accelerations of the floor were obtained from the acceleration signals recorded by the accelerometers installed at each floor level (shown in Fig. 9). The peak value was reported as the PFA when only one accelerometer was used in a single direction. For cases with multiple accelerometers in a single direction, the PFA was reported as the average of the peak values recorded by each accelerometer. Fig. 24 presents the horizontal PFAs at the Level 2 floor from which the fully-floating ceiling was suspended. The fully-floating ceiling was subjected simultaneously to a maximum demand of 0.60 g PFA in each horizontal direction (vector resultant of 0.85 g), under the bidirectional loading intensity of 0.88 g PGA (vector resultant of 1.25 g).

Table 2. Shaking sequence applied in the NSEs test phase.

Test No.	Intensity	% MCE	Target Peak Ground Acceleration, g		Remarks
			X	Y	
1	SLS-X	14	0.10	–	
2	SLS-Y	14	–	0.10	
3	SLS-XY1	10	0.07	0.07	
4	SLS-XY2	14	0.10	0.10	Inspection 1
5	2SLS-X	27	0.20	–	
6	2SLS-Y	27	–	0.20	
7	2SLS-XY1	19	0.14	0.14	
8	2SLS-XY2	27	0.20	0.20	Inspection 2
9	3SLS-X	41	0.30	–	
10	3SLS-Y	41	–	0.30	
11	3SLS-XY2	41	0.30	0.30	Inspection 3
12	ULS-X	55	0.40		Inspection 4
13	ULS-Y	55	–	0.40	Inspection 5
14	ULS-XY2	55	0.40	0.40	Inspection 6
15	1.2ULS-X	67	0.49		Inspection 7
16	1.2ULS-Y	67	–	0.49	Inspection 8
17	1.2ULS-XY2	67	0.49	0.49	Inspection 9
18	1.5ULS-X	82	0.60		Inspection 10
19	1.5ULS-Y	82	–	0.60	
20	1.5ULS-XY2	82	0.60	0.60	Inspection 11
21	MCE-XY1	100	0.73	0.73	
22	MCE-XY2	120	0.88	0.88	Inspection 12

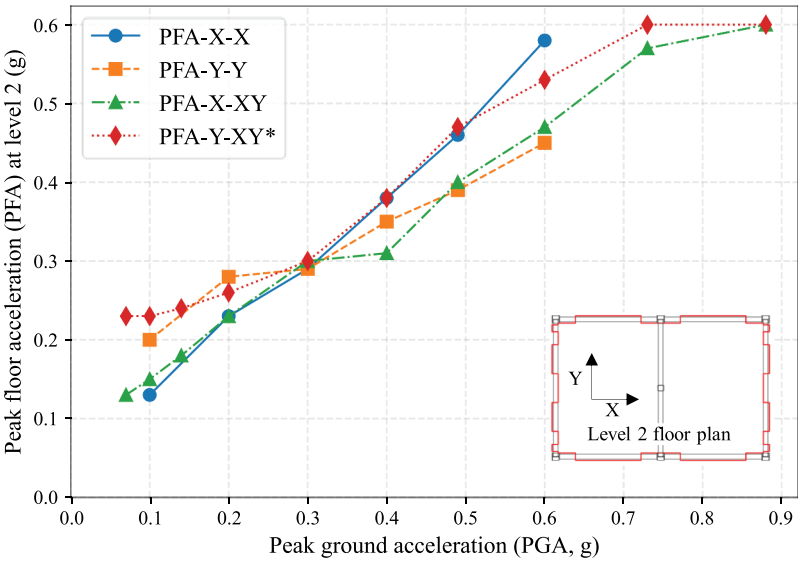

PFA-Y-XY*: PFA in Y-direction under bidirectional loading in X and Y directions.

Figure 24. PFA at level 2 of the test structure.

4.2. Natural Frequencies of the Fully-Floating Ceiling

The natural frequencies of the fully-floating ceiling were identified using frequency response functions (FRFs) computed from acceleration measurements. FRFs were obtained by taking the ratio of Fast Fourier Transform (FFT) (Arsac 1966) amplitudes of accelerations recorded by ceiling-mounted accelerometers to those recorded on the Level 2 floor under bidirectional white noise excitation in the X and Y directions. For the X-direction, the FRFs were obtained by using ceiling accelerometer

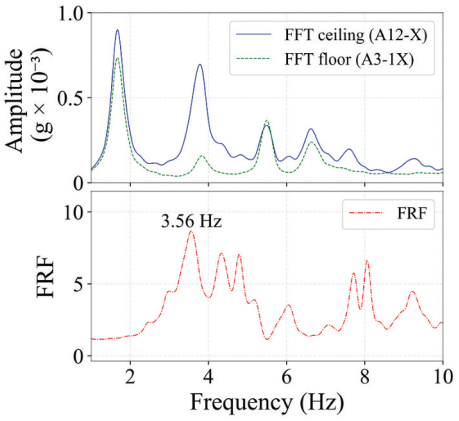

Figure 25. Fundamental natural frequency of the ceiling in the X-direction under the first white noise test, based on floor accelerometer A3-1X and ceiling accelerometer A12-X, conducted prior to the loading tests.

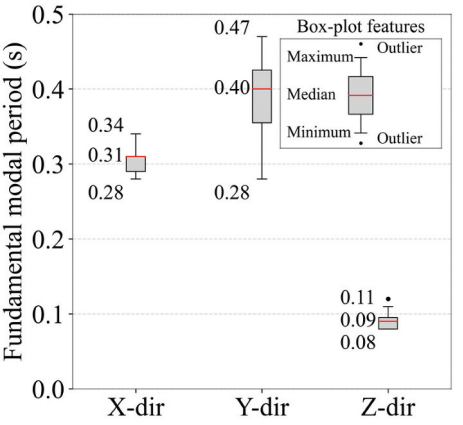

Figure 26. Fundamental modal periods of the fully-floating ceiling.

A12-X (Fig. 22) and floor accelerometers A3-1X and A3-3X (Fig. 9). Figure 25 shows the fundamental natural frequency of the ceiling in the X-direction under the first white noise test conducted prior to the commencement of the loading tests. Similarly, fundamental natural frequencies of the ceiling were identified in the Y and Z directions.

A summary of the ceiling's fundamental modal period is presented in the box-plot in Fig. 26. The median fundamental natural frequencies (and corresponding median fundamental modal periods) of the fully-floating ceiling were approximately 3.26 Hz (0.31 s), 2.50 Hz (0.40 s), and 11.54 Hz (0.09 s) in X, Y, and Z directions, respectively.

The natural frequencies of the fully-floating ceiling were also identified using FRFs utilizing the displacement signals under unidirectional loadings. In the X-direction, FRFs were computed using displacement records from ceiling-mounted string-potentiometers D17, D18, and D20 (Fig. 22), normalized by corresponding displacement records from floor-mounted string-potentiometers DX-3-1 and DX-3-2 (Fig. 9). Similarly, the natural frequencies in the Y-direction were identified, whereas those in the Z-direction could not be obtained due to the absence of vertical displacement measurements.

The median modal periods in the X and Y directions were 0.33 s and 0.43 s, respectively, in close agreement with those obtained from acceleration-based FRFs under white noise excitation. This agreement indicates that the ceiling response remained linear under the loading sequences, and supports the observation that the ceiling remained intact throughout the tests, as discussed in a later section. Nevertheless, modal periods identified under white noise excitation are reported herein, as white noise is a low-amplitude, broadband input specifically intended to excite the system within the linear range and to provide an estimate of its dynamic characteristics that is unbiased by the frequency content of the input excitation (Ewins 2000; Uhlig et al. 2023).

The modal period of a fully-floating ceiling (variant without isolation foam) is governed by the equation of a simple pendulum (Pourali et al. 2017; Robson et al. 2014; Yao 2000) expressed in Eq. (1):

$$T = 2\pi\sqrt{(L/g)} \tag{1}$$

Where, L is the length of the pendulum (ceiling plenum depth), and g is the acceleration due to gravity (9.81 m/s^2).

For a ceiling behaving as a simple pendulum with a plenum depth of 700 mm, equivalent to that of the ceiling investigated in this study, the theoretical modal period is 1.68 s. However, the modal period observed experimentally for the fully-floating ceiling in this study did not align with the simple

pendulum prediction. This discrepancy is attributed to the inclusion of isolation foam, which inhibits pendulum-like motion by introducing additional stiffness. Consequently, the modal period is better represented by a mass-spring system, as shown in Eq. (2):

$$T = 2\pi\sqrt{(m/k)} \tag{2}$$

Where, m is the mass of the ceiling, and k is the spring constant (representing the stiffness of the isolation foam).

Substituting the ceiling mass of 188 kg and the stiffness values of 61,342 N/m and 92,341 N/m in the X and Y directions, respectively, into Eq. (2), the modal periods were calculated to be 0.35 s in the X-direction and 0.28 s in the Y-direction. The stiffness values used in these calculations represent the initial stiffness of the isolation foam, based on the assumption that the initial stiffness governs the response under white noise excitation. These stiffness values correspond to the foam used in Pourali et al. (2017) as the foam employed in the current study is of a similar type.

Interestingly, the experimentally obtained modal periods are shorter in the X-direction and longer in the Y-direction than the respective theoretical estimates from Eq. (2), indicating a higher contribution of stiffness due to the isolation foam in the X-direction than in the Y-direction. This outcome can be attributed to the constraints encountered during the preparation and installation of the foam material, as detailed in the previous section. Furthermore, the isolation foam engaged with the screws connecting the seismic clips to the wall angle (shown in Fig. 18) at a spacing of 600 mm along the Y-direction edges, as the Tees were spaced at 600 mm along the Y-direction edges, whereas the spacing was at 1200 mm along the X-direction edges. This closer spacing of the screws engaging with the foam along the Y-direction edges increases the stiffness of the ceiling system in the X-direction because the extensive engagement along the Y-direction edges provides greater resistance to the ceiling movement along the X-direction. This effect, caused by unintended foam engagement, can be reduced by ensuring uniform foam width and using shorter screws.

4.3. Damping of the Fully-Floating Ceiling

Figure 27 presents a box-plot illustrating the damping ratios calculated using the Logarithmic Decrement Method (LDM) (Casiano 2016; Whetham 1890) and the Random Decrement Technique (RDT) (Casiano 2016; Cole 1968).

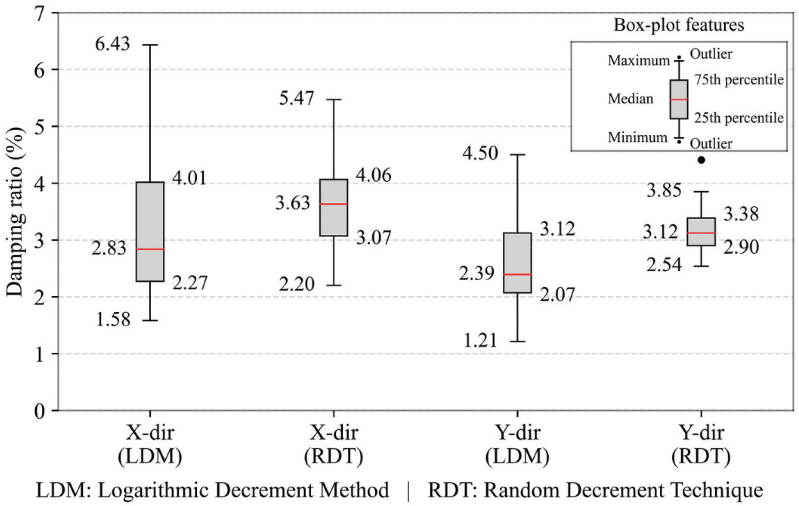

Figure 27. Damping ratios from experimental testing of the fully-floating ceiling.

For LDM, the free vibration decay region was manually extracted from the displacement signal for each loading sequence. According to Tweten, Ballard, and Mann (2014), using 3 to 22 peaks minimizes error in damping ratio estimation when damping ratio ranges between 0.01 and 0.10. Accordingly, appropriate segments of the free vibration decay were selected from each displacement record. In the X-direction, damping ratios were computed using displacement records from string-potentiometers D17, D18, and D20 (Fig. 22). For each record, damping ratios were evaluated using both positive and negative peaks, and the procedure was repeated for six unidirectional loading sequences (Table 2). An identical approach was applied in the Y-direction using displacement records from D19, D21, and D22.

For the RDT method, acceleration signals from white noise excitations were used. In the X-direction, damping ratios were calculated using the signal from accelerometer A12-X, while A12-Y was used for the Y-direction.

The average damping ratios reported by Pourali et al. (2017) range from 0.74% to 1.20%, based on free vibration tests of ceiling variants without isolation foam material. In contrast, the median damping ratios obtained in the current study (as shown in Fig. 27) range from 2.39% to 3.63%. These higher damping values correspond to ceiling configurations incorporating isolation foam, which restricts free motion. Accordingly, the higher damping ratios, observed in this study, which are approximately three times those reported by Pourali et al. (2017), align with the expected dampening effect of the isolation foam.

4.4. Displacement of the Fully-Floating Ceiling

Peak ceiling displacements shown in Fig. 28 correspond to the average of the maximum displacements from three string-potentiometers (Fig. 22), in the corresponding direction. Displacements in the Y-direction exceeded those in the X-direction, indicating that the ceiling system is stiffer in the X-direction than in the Y-direction. This observation supports the shorter fundamental modal period in the X-direction compared to the Y-direction, discussed in the previous section.

The maximum displacement experienced was 40.6 mm, which occurred at 0.60 g PFA in the Y-direction under bidirectional loading at a PGA of 0.88 g. According to the stress-strain curve

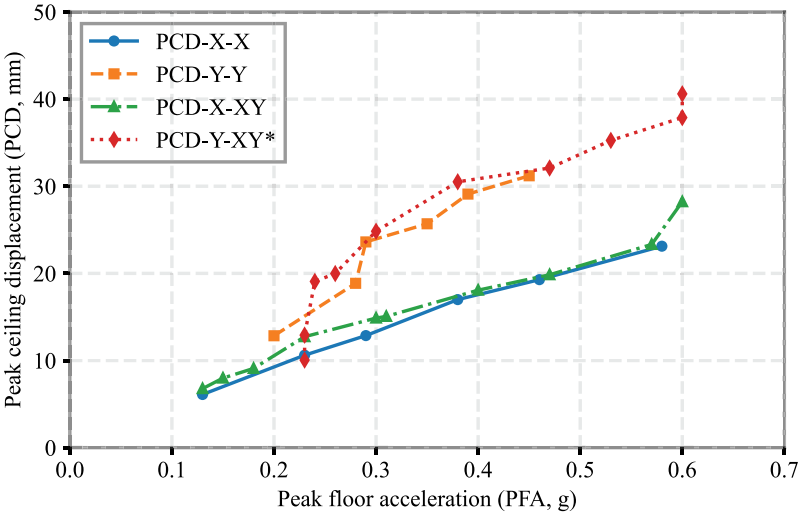

PCD-Y-XY*: PCD in Y-direction under bidirectional loading in X and Y directions.

Figure 28. Peak ceiling displacement.

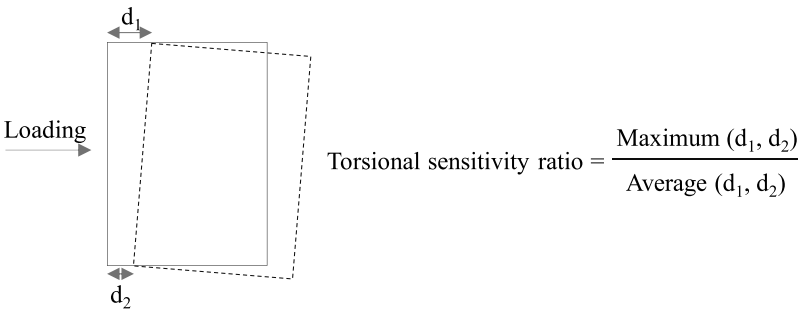

Figure 29. Schematic diagram showing torsional sensitivity ratio calculation.

reported by Pourali et al. (2017), the onset of densification of the foam material occurs at a strain level of approximately 0.80. Based on this, the minimum foam thickness required to accommodate the observed displacement is estimated to be 50 mm. Therefore, the installed 90 mm thick isolation foam was adequate to prevent pounding of the ceiling against surrounding elements in the tested building. In addition, peak ceiling displacements under bidirectional loading were nearly identical to those under unidirectional loading in both X and Y directions, suggesting that bidirectional loading condition has minimal influence on the displacement response of the fully-floating ceiling.

4.5. Torsional Sensitivity of Ceiling

Given that the fully-floating ceiling lacks braces and its perimeter edges are unrestrained, it may be susceptible to rotation about the vertical axis. Additionally, torsional sensitivity can arise from non-uniform foam thickness, as discussed in the previous section. Therefore, assessing the torsion sensitivity of the ceiling is essential. The torsional sensitivity ratio, defined in accordance with New Zealand technical specification, SNZ-TS-1170.5 (2025) is calculated as the ratio of the maximum end displacement in the loading direction to the average displacement of the two ends, as illustrated in Fig. 29. Torsional sensitivity ratios shown in Fig. 30 were obtained from peak displacements recorded by string potentiometers D17 and D18 (Fig. 22) in the X-direction, and by D21 and D22 in the Y-direction.

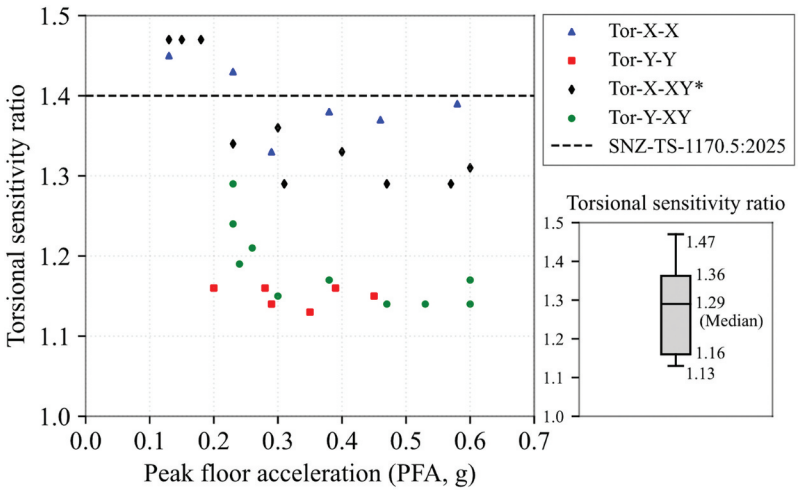

Figure 30. Torsional sensitivity ratio in the ceiling.

Currently, none of the publicly available design codes, such as SNZ-TS-1170.5 (2025) or research articles explicitly specify a limiting value for the torsional sensitivity ratio of suspended ceilings. However, no lay-in tiles exhibited local deformation in any direction (as discussed in a later section) owing to their mechanical attachment to the Tees using Velcro tape. Therefore, the ceiling system can reasonably be considered rigid within its plane. Under this assumption, the torsional sensitivity ratio shown in Fig. 30 can be compared with the threshold value of 1.40 recommended in SNZ-TS-1170.5 (2025) for assessing horizontal plan irregularities of rigid diaphragm due to torsional sensitivity. In a few loading cases, the torsional sensitivity ratio exceeded the limit of 1.40; however, no damage was observed in the ceiling. The median torsional sensitivity ratio value of 1.29 lies within this limit. Consequently, the ceiling system can be regarded as non-sensitive to torsional sensitivity (it is worth mentioning that the tested structure was also within the limit of torsional sensitivity ratio). As shown in Fig. 30, no clear trend is evident between unidirectional and bidirectional loadings; however, the torsional sensitivity ratio in the X-direction is higher than that in the Y-direction. This behaviour can be attributed to the asymmetric engagement of the foam along the X and Y direction edges. This effect can be reduced by ensuring uniform foam thickness and using shorter screws, as discussed earlier.

4.6. Acceleration in the Fully-Floating Ceiling

4.6.1. Amplification Factors Along the Horizontal Directions

The acceleration amplification factor (AAF) for the ceiling was calculated by dividing the peak ceiling acceleration by the corresponding peak floor acceleration for each loading case. In the X-direction, AAF was obtained using the ceiling-mounted accelerometer A12-X (Fig. 22) and floor-mounted accelerometers A3-1X and A3-3X (Fig. 9). In the Y-direction, AAF was similarly calculated using ceiling-mounted accelerometer A12-Y and floor-mounted accelerometers A3-1Y, and A3-3Y. The data did not show any consistent trend between unidirectional and bidirectional loadings, or between X and Y directions. The resulting AAFs, shown in Fig. 31, under unidirectional and bidirectional horizontal shaking range from 1.13 to 2.80, with a median value of 2.16. These values are within the limit of 4 specified by SNZ-TS-1170.5 (2025) for flexible components mounted above ground level.

4.6.2. Vertical Peak Component Ceiling Acceleration

The vertical peak floor acceleration (PFA-Z) was obtained from a single accelerometer (A3-2Z), installed in the Z-direction near the geometric center of the Level 2 floor (Fig. 9). Vertical peak component ceiling accelerations (PCA-Zs) were obtained from accelerometers A12-Z, A13-Z, and A14-Z (Fig. 22). Among these, A12-Z is positioned near the geometric center of the ceiling, A13-Z is positioned closer to the edge, and A14-Z is positioned near the

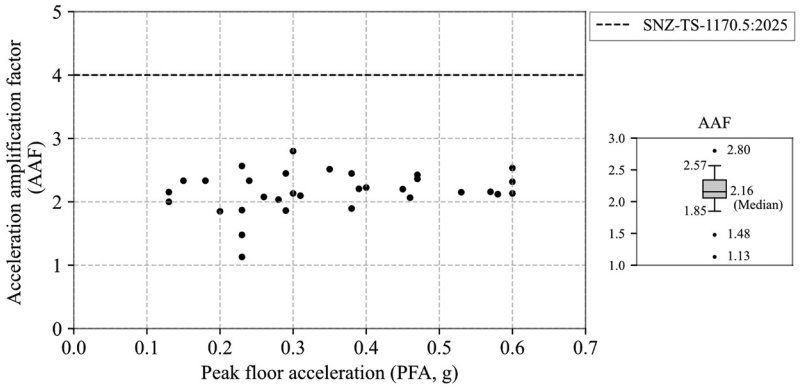

Figure 31. Acceleration amplification factors in the horizontal directions.

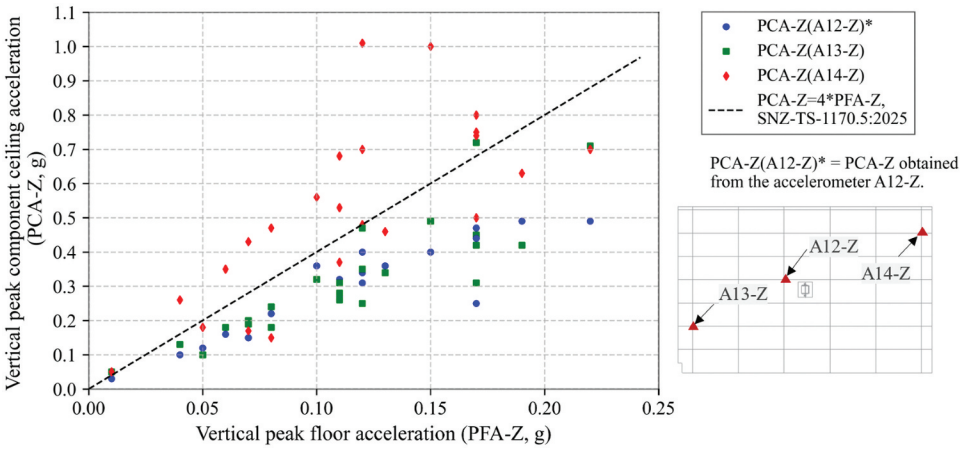

Figure 32. Peak component ceiling acceleration in the Z-direction.

corner. PCA-Z obtained from accelerometer A14-Z was the highest in most loading cases and is shown as PCA-Z (A14-Z) in Fig. 32.

The highest PCA-Z observed was 1.01 g (i.e. including gravity 2.01 g) at the corner of the ceiling, obtained from A14-Z accelerometer. As shown in Fig. 32, approximately one-fourth of the PCA-Z values exceeded four times the corresponding PFA-Z, thereby surpassing the limit specified by SNZ-TS-1170.5 (2025). All these data points correspond to the PCA-Z of the corner of the ceiling, obtained from A14-Z accelerometer. This implies that the vertical peak component ceiling acceleration can vary across different ceiling locations. Therefore, if a conservative value is to be used for design purposes, it should correspond to the location farthest from the centre, typically at the ceiling corner.

5. Damage Observed in the Fully-Floating Ceiling

The fully-floating ceiling system demonstrated no damage to any of its components throughout the loading sequences and remained intact as observed prior to testing (as shown in Figs. 20 and 21). Failures, such as tile dislodgement, Tee deformation, hanger wire detachment, wall angle compromise or tearing of the lay-in tiles due to pounding with droppers were not observed during the entire testing program.

In the shake table tests conducted by Jun et al. (2022) on a freely suspended lay-in tile ceiling system measuring 3870 mm by 3870 mm and supported solely by hanger wires, approximately 30% of the lay-in tiles became dislodged. The maximum vertical acceleration amplification of the ceiling was approximately 4.5. In contrast, the present study observed a maximum vertical acceleration amplification of 8.4. However, none of the lay-in tiles were dislodged, suggesting that the Velcro tape effectively secured the tiles to the Tees.

The sprinkler heads attached to flexible droppers also exhibited no pounding against the lay-in tiles. The support bar clamped the flexible droppers to the Tees, thereby preventing any relative movement and subsequent tearing of the lay-in tiles.

6. Conclusions

A low-damage fully-floating ceiling with foam edging was installed on the second-floor level of a full-scale, three-storey steel-framed building that was subjected to shake table testing

under unidirectional and bidirectional shaking as part of the NZ-China collaborative ROBUST project at ILEE. The lay-in tiles of these ceilings were secured using Velcro tape, between the lay-in tiles and the Tees seating the lay-in tiles. This is a novel approach to prevent dislodgement and collapse of lay-in tiles, which has been a common occurrence leading to ceiling collapses in past earthquakes. The ceiling was subjected to a maximum of 0.60 g PFA (vector resultant of 0.85 g) in the horizontal directions under bidirectional loading intensity of 0.88 g PGA (vector resultant of 1.25 g). Based on the study, the following conclusions are drawn for the tested fully-floating ceiling with Velcro-secured lay-in tiles:

(1) The median fundamental natural periods ranged from 0.31 s to 0.40 s.
(2) The median damping ratios ranged from 2.39% to 3.63%.
(3) The maximum ceiling displacement recorded under seismic loading conditions was 40.6 mm.
(4) The median torsional sensitivity ratio was 1.29, which is within the limit of 1.40, specified by SNZ-TS-1170.5 (2025). Accordingly, the ceiling was deemed insensitive to torsional sensitivity.
(5) The acceleration amplification factors in the horizontal directions ranged from 1.13 to 2.80, with a median value of 2.16. These values fall within the permissible limit of 4, as specified by SNZ-TS-1170.5 (2025) for flexible components mounted above ground level.
(6) The maximum vertical peak ceiling acceleration recorded was 1.01 g. The vertical peak component ceiling acceleration was observed to vary across different ceiling locations, with the highest values typically occurring at the corners. Therefore, for conservative design purposes, the value corresponding to the location farthest from the centre, typically at the ceiling corner, should be used.
(7) No pounding between the sprinkler heads and the lay-in tiles was observed during testing. This demonstrates that flexible droppers are compatible with the fully-floating ceiling system.
(8) No damage was observed in any of its components throughout the loading sequences.
(9) The method of securing lay-in tiles to the Tees using Velcro tape proved to be both feasible and practical, requiring no specialized tools or procedures. This highlights its strong potential for real-world application.

Overall, the study underscores the fully-floating ceiling system featuring Velcro-secured lay-in tiles as a resilient and low-damage ceiling solution for buildings in earthquake-prone regions.

Acknowledgments

The work described was conducted as part of a joint NZ-China research programme with the International Laboratories on Earthquake Engineering (ILEE), Tongji University, Shanghai, China, and directly with Tongji University, Shanghai, China. Direct NZ funding is kindly provided by the Building Research Association of NZ (BRANZ) under the Building Research Levy, EQC Toka Tū Ake, the HERA Foundation (a charitable trust associated with the Heavy Engineering Research Association), the Building Innovation Partnership, the Tertiary Education Commission funded QuakeCoRE (the NZ ILEE partner through whom the NZ funding is also coordinated), and the University of Auckland (UA). Administrative and personnel support is also provided by Auckland University of Technology (AUT), University of Canterbury, and the NZ Ministry of Business, Innovation and Employment, Endeavour Programme on Sustainable Earthquake Resilient Buildings for a Better Future - PROP-83779-ENDRP-AUT). Donations of materials are provided by ComFlor, Hilti Corporation, Tracklok, Gripple, Lanyon & LeCompte Construction Ltd., and Alutech Doors & Windows Ltd. Expertise has been generously provided by a number of Chinese and NZ industry representatives. The authors gratefully acknowledge this support. We would like to sincerely thank the RObust BUilding SysTem Project team for their support. Opinions expressed are those of the authors alone. This is QuakeCoRE publication number 1113.

Author Contributions

CRediT: **A. Tiwari:** Conceptualization, Data curation, Formal analysis, Investigation, Methodology, Software, Validation, Visualization, Writing – original draft, Writing – review & editing; **J. Bhatta:** Resources, Supervision, Validation, Writing – review & editing; **R. P. Dhakal:** Conceptualization, Funding acquisition, Project administration,

Resources, Supervision, Validation, Writing – review & editing; **T. J. Sullivan:** Supervision, Writing – review & editing; **R. K. Shrestha:** Investigation, Writing – review & editing; **Z. Yan:** Project administration, Resources, Writing – review & editing; **G. A. MacRae:** Funding acquisition, Project administration, Writing – review & editing; **J. Yu:** Investigation, Writing – review & editing; **P. Xiang:** Funding acquisition, Project administration, Writing – review & editing; **M. Rashid:** Resources, Writing – review & editing; **Y. Zhang:** Investigation, Writing – review & editing; **L. Jia:** Funding acquisition, Project administration, Writing – review & editing; **S. Ramhormozian:** Funding acquisition, Project administration, Writing – review & editing; **G. C. Clifton:** Funding acquisition, Project administration, Writing – review & editing; **P. Quenneville:** Funding acquisition, Project administration, Writing – review & editing; **G. Rodgers:** Funding acquisition, Project administration; **X. Zhao:** Funding acquisition, Project administration.

Disclosure Statement

No potential conflict of interest was reported by the author(s).

ORCID

R. P. Dhakal http://orcid.org/0000-0001-5524-5919

Data Availability Statement

The data that support the findings of this study are available from the corresponding author [AT] upon reasonable request.

References

ANCO-Engineers-Inc. 1983. *Seismic Hazard Assessment of Non-Structural Ceiling Components: Phase I. [Grant 8114155]*. National Science Foundation.

Arsac, J. 1966. *Fourier Transforms and the Theory of Distributions*. Englewood Cliffs, N.J: Prentice-Hall.

Badillo-Almaraz, H., A. S. Whittaker, and A. M. Reinhorn. 2007. "Seismic Fragility of Suspended Ceiling Systems." *Earthquake Spectra* 23 (1): 21–40. https://doi.org/10.1193/1.2357626.

Bagheri, H. 2022. "Seismic Performance of a Full-Scale Steel Structure Using Resilient Slip Friction Joints." PhD Dissertation, Auckland, New Zealand: Department of Civil and Environmental Engineering, The University of Auckland. https://hdl.handle.net/2292/60019.

Bhatta, J., and R. P. Dhakal. 2026. "Seismic Response Assessment of "Rocking" Interior Partition Walls with Dual-Slot Tracks Under Different Construction Details." *Journal of Earthquake Engineering*: 1–25. https://doi.org/10.1080/13632469.2025.2612533.

Bhatta, J., R. P. Dhakal, T. J. Sullivan, and M. Lanyon. 2022. "Low-Damage Rocking Precast Concrete Cladding Panels: Design Approach and Experimental Validation." *Journal of Earthquake Engineering* 26 (9): 4387–4420. https://doi.org/10.1080/13632469.2020.1830201.

Bianchi, S., J. Ciurlanti, D. Perrone, A. Filiatrault, A. C. Costa, P. X. Candeias, A. A. Correia, and S. Pampanin. 2021. "Shake-Table Tests of Innovative Drift Sensitive Nonstructural Elements in a Low-Damage Structural System." *Earthquake Engineering and Structural Dynamics* 50 (9): 2398–2420. https://doi.org/10.1002/eqe.3452.

Bradley, B. A., R. P. Dhakal, M. Cubrinovski, G. A. MacRae, and D. S. Lee. 2009. "Seismic Loss Estimation for Efficient Decision Making." *Bulletin of the New Zealand Society for Earthquake Engineering* 42 (2): 96–110. June 30. https://doi.org/10.5459/bnzsee.42.2.96-110.

Browne, M., J. Long, and J. Stanway. 2024. *Recommended Practice for Seismic Restraint Design of Suspended Ceilings*. Wellington, New Zealand: New Zealand Society for Earthquake Engineering. https://repo.nzsee.org.nz/handle/nzsee/2710.

Casiano, M. J. 2016. *Extracting Damping Ratio from Dynamic Data and Numerical Solutions*. Huntsville, Alabama: National Aeronautics and Space Administration (NASA).

Cole, H. A., Jr. 1968. "On-the-Line Analysis of Random Vibrations." In *AIAA/ASME 9th Structural Dynamics and Materials Conference*, Palm Springs, USA, 1–8. American Institute of Aeronautics and Astronautics. AIAA Paper No. 68-288.

Dhakal, R. 2024. "Seismic Design of Buildings: Where to Next?" *Bulletin of the New Zealand Society for Earthquake Engineering* 57 (1): 1–17. https://doi.org/10.5459/bnzsee.1680.

Dhakal, R. P. 2010. "Damage to Non-Structural Components and Contents in 2010 Darfield Earthquake." *Bulletin of the New Zealand Society for Earthquake Engineering* 43 (4): 404–411. https://doi.org/10.5459/bnzsee.43.4.404-411.

Dhakal, R. P., G. A. MacRae, and K. Hogg. 2011. "Performance of Ceilings in the February 2011 Christchurch Earthquake." *Bulletin of the New Zealand Society for Earthquake Engineering* 44 (4): 377–387. https://doi.org/10.5459/bnzsee.44.4.377-387.

Dhakal, R. P., G. A. Macrae, A. Pourali, and G. Paganotti. 2016. "Seismic Fragility of Suspended Ceiling Systems Used in NZ Based on Component Tests." *Bulletin of the New Zealand Society for Earthquake Engineering* 49 (1): 45–63. https://doi.org/10.5459/bnzsee.49.1.45-63.

Dhakal, R. P., M. Rashid, J. Bhatta, C. Chen, G. Q. Song, T. J. Sullivan, G. A. Macrae, G. C. Clifton, P. Xiang, and L. J. Jia. 2020. "Shake T Able Testing Plan for Multiple Non-Structural Elements and Contents in a Low-Damage Structural Steel Building." In *17th World Conference on Earthquake Engineering, 17WCEE*, Sendai, Japan, 1–12. WCEE.

Ditommaso, R., N. Lamarucciola, and F. C. Ponzo. 2024. "Prediction of the Fundamental Period of Infilled RC Framed Structures Considering the Maximum Inter-Story Drift at Different Design Limit States." *Structures* 63:106422. https://doi.org/10.1016/j.istruc.2024.106422.

Ditommaso, R., F. Scozzese, A. Zona, A. Dall'asta, and F. C. Ponzo. 2025. "Shake-Table Tests for Seismic Performance Assessment of Glass-Aluminium Partition Walls with Viscoelastic Dissipative Devices." *Journal of Earthquake Engineering*: 1–24. https://doi.org/10.1080/13632469.2025.2525919.

Ewins, D. J. 2000. *Modal Testing: Theory, Practice and Application*. Hertfordshire, England: Research Studies Press Ltd.

FEMA356. 2000. *Prestandard and Commentary for the Seismic Rehabilitation of Buildings*. Federal Emergency Management Agency (FEMA). https://www.nehrp.gov/pdf/fema356.pdf .

Gilani, A. S. J., M. Reinhorn Andrei, B. Glasgow, O. Lavan, and H. K. Miyamoto. 2010. "Earthquake Simulator Testing and Seismic Evaluation of Suspended Ceilings." *Journal of Architectural Engineering* 16 (2): 63–73. https://doi.org/10.1061/(ASCE)1076-0431(2010)16:2(63).

Jun, S.-C., C.-H. Lee, C.-J. Bae, and K.-J. Lee. 2022. "Shake-T Able Seismic Performance Evaluation of Direct- and Indirect-Hung Suspended Ceiling Systems." *Journal of Earthquake Engineering* 26 (9): 4833–4851. https://doi.org/10.1080/13632469.2020.1845876.

Khakurel, S., R. P. Dhakal, T. Z. Yeow, and S. K. Saha. 2020. "Performance Group Weighting Factors for Rapid Seismic Loss Estimation of Buildings of Different Usage." *Earthquake Spectra* 36 (3): 1141–1165. https://doi.org/10.1177/8755293019901311.

MacRae, G. A., X. Zhao, L. Jia, G. C. Clifton, R. Dhakal, P. Xiang, S. Ramhormozian, and G. Rodgers. 2020. "The China-NZ ROBUST Friction Building Shaking T Able Testing Overview." In *The 17th World Conference on Earthquake Engineering*, Japan, 1–10. WCEE. https://ir.canterbury.ac.nz/bitstreams/91612e40-fe1c-4336-bf25-f515416a4686/download.

MacRae, G., L.-J. Jia, Z. Yan, C. Clifton, S. Ramhormozian, R. Dhakal, P. Xiang, G. Rodgers, P. Quenneville, and X. Zhao. 2024. "The Robust Steel Building Response." In *NZSEE 2024 Annual Conference*, Wellington, New Zealand, 1–14. NZSEE. https://repo.nzsee.org.nz/bitstream/handle/nzsee/2675/MacRae5.pdf?sequence=1&isAllowed=y.

Maneetes, H., and A. M. Memari. 2014. "Introduction of an Innovative Cladding Panel System for Multi-Story Buildings." *Buildings* 4 (3): 418–436. https://doi.org/10.3390/buildings4030418.

Motosaka, M., and K. Mitsuji. 2012. "Building Damage During the 2011 Off the Pacific Coast of Tohoku Earthquake." *Soils & Foundations* 52 (5): 929–944. https://doi.org/10.1016/j.sandf.2012.11.012.

Mulligan, J., T. J. Sullivan, and R. P. Dhakal. 2022. "Experimental Seismic Performance of Partly-Sliding Partition Walls." *Journal of Earthquake Engineering* 26 (3): 1630–1655. https://doi.org/10.1080/13632469.2020.1733139.

NZS1170.5. 2016. *Structural Design Actions, Part 5: Earthquake Actions—New Zealand (NZS 1170.5:2004)*. Standards New Zealand. https://www.standards.govt.nz/shop/NZS-1170-5-SUPP-12004-INCLUDES-AMDT-1.

Pinelli, J. P., C. Moor, J. I. Craig, and B. J. Goodno. 1996. "Testing of Energy Dissipating Cladding Connections." *Earthquake Engineering and Structural Dynamics* 25 (2): 129–147. https://doi.org/10.1002/(SICI)1096-9845(199602)25:2.

Pourali, A., R. P. Dhakal, G. Macrae, and A. S. Tasligedik. 2017. "Fully Floating Suspended Ceiling System: Experimental Evaluation of Structural Feasibility and Challenges." *Earthquake Spectra* 33 (4): 1627–1654. https://doi.org/10.1193/092916EQS163M.

Rashid, M. 2022. "Seismic Assessment and Design of Fire Sprinkler Piping System." PhD Dissertation, Christchurch, New Zealand: Department of Civil and Natural Resources Engineering, University of Canterbury. https://doi.org/10.26021/12872.

Robson, M. J., D. N. Kho, A. Pourali, and R. P. Dhakal. 2014. "Feasibility of a Fully Floating Ceiling System." In *New Zealand Society for Earthquake Engineering Conference*, Auckland, NZ. March 21–23, 1–9. NZSEE.

Ryu, K. P., and A. M. Reinhorn. 2019. "Experimental Study of Large Area Suspended Ceilings." *Journal of Earthquake Engineering* 23 (6): 1001–1032. https://doi.org/10.1080/13632469.2017.1342294.

SNZ-TS-1170.5. 2025. *Standards New Zealand Technical Specification*. Standards New Zealand. https://www.standards.govt.nz/shop/snz-ts-1170-52025.

Soroushian, S., E. M. Maragakis, and C. Jenkins. 2015. "Capacity Evaluation of Suspended Ceiling Components, Part 1: Experimental Studies." *Journal of Earthquake Engineering* 19 (5): 784–804. https://doi.org/10.1080/13632469.2014.998354.

Soroushian, S., L. Ryan Keri, M. Maragakis, E. Sato, T. Sasaki, T. Okazaki, L. Tedesco, E. Zaghi Arash, G. Mosqueda, and D. Alvarez. 2012. "Seismic Response of Ceiling/Sprinkler Piping Nonstructural Systems in NEES TIPS/NEES Nonstructural/NIED Collaborative Tests on a Full Scale 5-Story Building." In *Structures Congress 2012*, 1315–1326. ASCE. Accessed January 18, 2025. https://doi.org/10.1061/9780784412367.118.

Steel & Tube. 2016. "ComFlor®80 Product Guide." https://steelandtube.co.nz/sites/default/files/catalogues/Comflor80_PG-Dec2016-01.pdf.

Su, R. K. L., A. M. Chandler, M. N. Sheikh, and N. T. K. Lam. 2005. "Influence of Non-Structural Components on Lateral Stiffness of Tall Buildings." *The Structural Design of Tall & Special Buildings* 14 (2): 143–164. https://doi.org/10.1002/tal.266.

Taghavi, S., and M. M. Miranda. 2003. *Response Assessment of Nonstructural Building Elements*. (2003/05). Pacific Earthquake Engineering Research Center, College of Engineering, University of California Berkeley.

Tweten, D. J., Z. Ballard, and B. P. Mann. 2014. "Minimizing Error in the Logarithmic Decrement Method Through Uncertainty Propagation." *Journal of Sound and Vibration* 333 (13): 2804–2811. June 23. https://doi.org/10.1016/j.jsv.2014.02.024.

Uhlig, S., I. Alkhasli, F. Schubert, C. Tschöpe, and M. Wolff. 2023. "A Review of Synthetic and Augmented Training Data for Machine Learning in Ultrasonic Non-Destructive Evaluation." *Ultrasonics* 134:107041. September 1. https://doi.org/10.1016/j.ultras.2023.107041.

Velcro-Brand. n.d. "VELCRO® Brand Heavy-Duty Mounting Tape." https://www.velcro.com/products/garage-organization/velcro-brand-extreme-outdoor-tape/.

Whetham, W. 1890. "On the Alleged Slipping at the Boundary of a Liquid in Motion." *Philosophical Transactions of the Royal Society of London* 181 (181): 559–582. https://doi.org/10.1098/rsta.1890.0010.

Yagi, S., A. Teramoto, T. Yeow, T. Seike, K. Kusunoki, and I. Nakamura. 2022. "Validating Resilient Detailing of Japanese Ceilings, Windows, and Wall Tiles Using an E-Defense Shake-Table Test." *Journal of Earthquake Engineering* 26 (16): 8525–8551. https://doi.org/10.1080/13632469.2021.1988764.

Yan, Z., S. Ramhormozian, G. C. Clifton, G. MacRae, G. Rodgers, P. Quenneville, R. Dhakal, P. Xiang, L. J. Jia, and X. Zhao. 2024. "Shake Table Testing of a Low-Damage Steel Frame Building Incorporating Asymmetric and Symmetric Friction Connections." In *Proceedings of the 11th International Conference on Behaviour of Steel Structures in Seismic Areas*, Salerno, Italy, edited by F. M. Mazzolani, V. Piluso, E. Nastri, and A. Formisano, Vol. 519, 607–616. Springer Nature Switzerland. https://doi.org/10.1007/978-3-031-62884-9_53.

Yan, Z., S. Ramhormozian, G. C. Clifton, R. Zhang, P. Xiang, L.-J. Jia, G. A. MacRae, and X. Zhao. 2023. "Numerical Studies on the Seismic Response of a Three-Storey Low-Damage Steel Framed Structure Incorporating Seismic Friction Connections." *Resilient Cities and Structures* 2 (1): 91–102. https://doi.org/10.1016/j.rcns.2023.02.007.

Yao, G. C. 2000. "Seismic Performance of Direct Hung Suspended Ceiling Systems." *Journal of Architectural Engineering* 6 (1): 6–11. March 1. https://doi.org/10.1061/(ASCE)1076-0431(2000)6:1(6).

Zaghi, A. E., S. Soroushian, A. Echevarria Heiser, M. Maragakis, and A. Bagtzoglou. 2016. "Development and Validation of a Numerical Model for Suspended-Ceiling Systems with Acoustic Tiles [Article]." *Journal of Architectural Engineering* 22 (3): Article 04016008. https://doi.org/10.1061/(ASCE)AE.1943-5568.0000213.